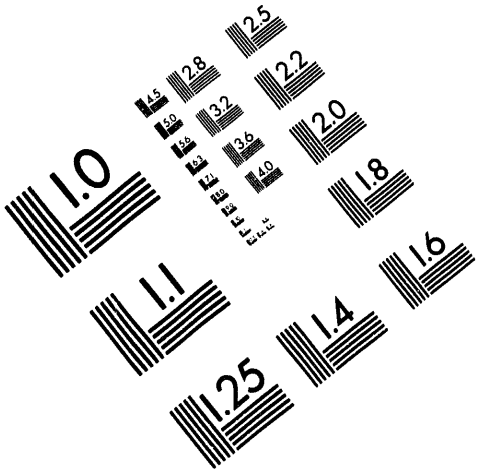

Association for Information and Image Management

1100 Wayne Avenue, Suite 1100
Silver Spring, Maryland 20910

301/587-8202

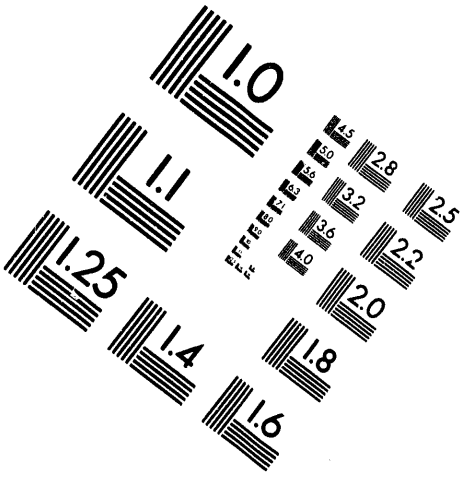

Centimeter

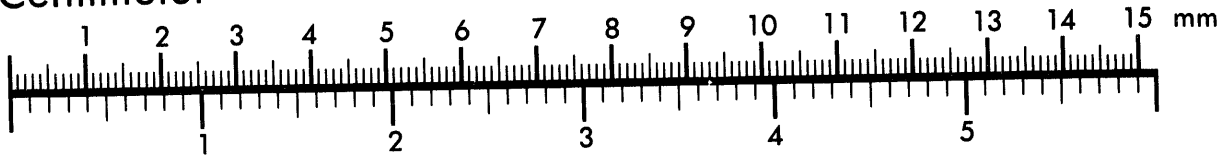

Inches

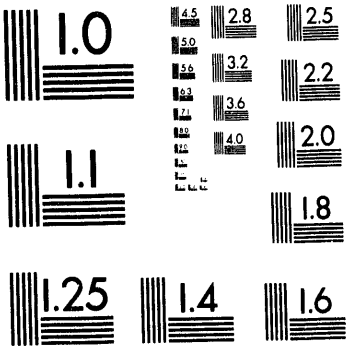

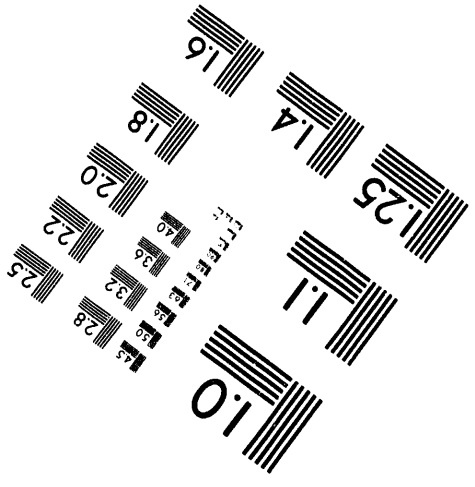

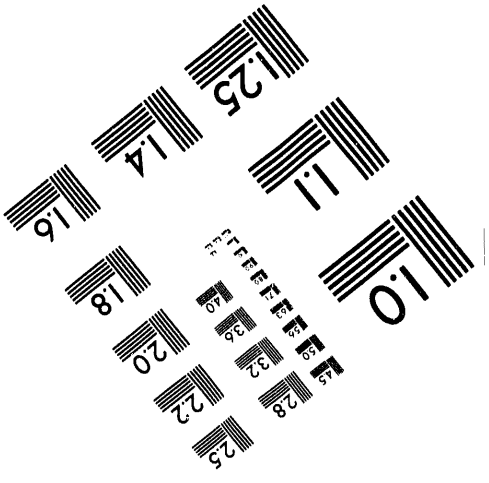

MANUFACTURED TO AIIM STANDARDS
BY APPLIED IMAGE, INC.

1 of 1

Excitation of Alfvén Cyclotron Instability by Charged Fusion Products in Tokamaks

N. N. Gorelenkov*and C. Z. Cheng

Princeton Plasma Physics Laboratory, Princeton University

P. O. Box 451, Princeton, New Jersey 08543 USA

Abstract

The spectrum of ion cyclotron emission (ICE) observed in tokamak experiments shows narrow peaks at multiples of the edge cyclotron frequency of background ions. A possible mechanism of ICE based on the fast Alfvén Cyclotron Instability (ACI) resonantly excited by high energy charged products (α-particles or protons) is studied here. The two-dimensional ACI eigenmode structure and eigenfrequency are obtained in the large tokamak aspect ratio limit. The ACI is excited via wave-particle resonances in phase space by tapping the fast ion velocity space free energy. The instability growth rates are computed perturbatively from the perturbed fast particle distribution function, which is obtained by integrating the high frequency gyrokinetic equation along the particle orbit. Numerical examples of ACI growth rates are presented for TFTR plasmas. The fast ion distribution function is assumed to be singular in pitch angle near the plasma edge. The results are employed to understand the ICE in Deuterium-Deuterium (DD) and Deuterium-Tritium (DT) tokamak experiments.

*Permanent address: Troitsk Institute for Innovative and Fusion Research, Troitsk, Moscow region, Russia, 142092

MASTER

DISTRIBUTION OF THIS DOCUMENT IS UNLIMITED

I. INTRODUCTION

New observational results of Ion Cyclotron Emission (ICE) on TFTR[1,2] and JET[3,4] (see also references contained therein) near plasma edge have been reported recently. The measured ICE frequency spectra in Deuterium-Deuterium (DD) and Deuterium-Tritium (DT) discharges show peaks at multiple harmonics of deuterium cyclotron frequency $l\omega_{cD}$ (and/or harmonics of tritium cyclotron frequency- $l\omega_{cT}$ for DT) evaluated at the outer periphery of the plasma. The width of each peak is very narrow with $\Delta\omega/\omega \ll a/R$ and $l \leq 10$, where a and R are the minor and major radii of the tokamak plasma, respectively. The results indicate that ICE is localized spatially near the plasma edge, and there is strong evidence that ICE is driven by charged fusion products. A linear correlation between the ICE power and neutron emission rate over six orders of magnitude was observed in JET.[3] ICE spectrum is more complicated in TFTR. In ohmically heated DD discharges, a different set of lines in the ICE spectra, corresponding to the odd deuteron harmonics, $\omega = (2l+1)\omega_{cD}$, were observed. For higher frequencies around $\omega = 10\omega_{cD}$ a broadband emission was also observed. The ICE spectrum intensity was found to be proportional to the evolving neutron emission.[1] In TFTR DT discharges,[2] ICE spectrum was observed at the initial stage of NBI, with ICE peak frequencies corresponding to the α- particle (deuterium) edge cyclotron frequency. During the steady state NBI heating the ICE spectrum presents a rather complicated picture of the peaks located at tritium and/or deuterium cyclotron frequencies. These observations also show a correlation of ICE intensity with the neutron emission rate. Thus, the ICE can be employed as a diagnostic tool to investigate the properties of fast ion population and the plasma, at least near the plasma edge.

Recent theoretical investigations[5-9] considered ICE to be the Alfvén Cyclotron Instabil-

ity (ACI) driven by fast charged fusion ions which are in cyclotron resonance with the fast compressional Alfvén wave. In papers[5–7] the instability was studied in the uniform plasma approximation. In papers[8,9] the two-dimensional eigenmode structure was obtained in the large aspect ratio limit ($\epsilon = a/R \ll 1$), but a local analysis of the wave - particle interaction was performed. The possibility of exciting ACI with very low fast particle density was demonstrated. However, this theory cannot explain the instabilities at low cyclotron harmonic frequencies, especially for the DT case with $v_{\alpha 0}/v_A \simeq 1$, where $v_{\alpha 0}$ is the α-particle birth velocity, and v_A is the Alfvén velocity. One overly restrictive condition for the uniform plasma theory[5–7] to be correct, requires that the instability growth rate $\gamma \gg \omega_{b\alpha}$, where $\omega_{b\alpha}$ is the α-particle bounce frequency. This condition requires much higher α-particle density than typical experimental values near the plasma edge.

The theory of cyclotron thermonuclear instability was developed earlier[10] (see references therein). It included the drift motion of fast particles, but the fast particle finite orbit width was assumed negligible in comparison with the radial wavelength. The analytical theory reviewed in[10] cannot be applied directly to the experiments. One reason is that the radial excursions of fast particle orbit in TFTR and JET are comparable to the minor radius. The second reason is that the final growth rate expression contains high bounce harmonic resonances and requires numerical evaluation due to complicated, nonlocal resonance condition along the particle orbit.

In this paper we will consider the excitation mechanism of ICE based on ACI driven by fast particles. Our aim is to develop a two dimensional formalism for fast particle - compressional Alfvén wave interaction and to show that ACI can be unstable to explain the ICE observation in TFTR and JET experiments. The structure and the spectrum of compressional Alfvén eigenmodes are obtained by neglecting ion FLR effects and plasma pressure in

the large aspect ratio limit. The growth rates due to fast ions are computed perturbatively from the perturbed fast ion distribution function, which is obtained by integrating the high frequency gyrokinetic equation along the particle orbit. The equilibrium fast ion velocity distribution function is asumed to be singular in pitch angle.

To excite the ACI the growth rate due to fast ions must be higher than all dampings due to thermal electrons and ions. To minimize such dampings and to find the most unstable eigenmodes we will mainly consider modes with small parallel component of the wave vector $k_{\|}$ in comparison with perpendicular component $k_{\perp}$. Electron Landau damping can be avoided by choosing $k_{\|} \ll \omega/v_{Te}$, i.e., the wave phase velocity is higher than the electron thermal velocity.[8,11] Thermal ions can contribute to significant cyclotron damping at $\omega/\omega_{ci} \sim 1$. However, the thermal ion damping can be minimized for eigenmodes that are radially localized near the plasma edge, where the thermal ion density and temperature are small. At higher cyclotron harmonic frequencies the thermal ion damping is exponentially small. We also note that in tokamak devices such as TFTR or JET the fast ions have radial drift orbit excursion comparable to the minor radius. It leads to high anisotropy in their velocity space distribution which provides free energy to destabilize the ACI. The velocity space anisotropy of the α-particle distribution is a function of the α-particle source gradient and is higher near the plasma edge.[12] Thus, radially localized eigenmodes located in the region of high velocity space anisotropy and large fast ion population will be most easily excited. Such eigenmodes are responsible for the measured ICE spectrum peaks.

The paper is organized as follows. In Sec. II we present a two dimensional eigenmode analysis for compressional Alfvén eigenmode structure and eigenfrequency, and a perturbative analysis for fast particle contributions. In Section III the kinetic fast particle contribution is obtained in a WKB approximation by solving a general frequency gyrokinetic equation.

Sec. IV deals with numerical calculations of ACI growth rates using the perturbative method. A summary is given in Sec. V.

II. COMPRESSIONAL ALFVÉN WAVE DISPERSION

A. Eigenmode equation

We will look for electromagnetic modes in the ion cyclotron frequency range, and the compressional Alfvén wave is a possible candidate. To obtain the compressional Alfvén wave eigenmode solution, we neglect the fast ion kinetic effects and consider the model of inhomogeneous, magnetized plasma in a simple toroidal configuration with a circular cross section and large aspect ratio. In the absence of kinetic contribution from wave-particle interactions, the eigenmode equation is determined by the cold plasma dispersion relation

$$k^2 = \frac{\epsilon_2^2}{k_{\|}^2 - \epsilon_1} + \epsilon_1, \tag{1}$$

where

$$\epsilon_1 = \frac{\omega^2}{c^2}\hat{\epsilon}_{11} = \frac{\omega^2}{c^2}\hat{\epsilon}_{22} = \sum_i \frac{\omega_{pi}^2/c^2}{\omega_{ci}^2/\omega^2 - 1},$$
$$\epsilon_2 = -i\frac{\omega^2}{c^2}\hat{\epsilon}_{12} = i\frac{\omega^2}{c^2}\hat{\epsilon}_{21} = \sum_i \frac{\omega}{\omega_{ci}} \frac{\omega_{pi}^2/c^2}{\omega_{ci}^2/\omega^2 - 1},$$

ω_{ci} and ω_{pi} are the cyclotron and plasma frequencies of ion species i, k is the wavevector, and $\hat{\epsilon}_{ij}$ are elements of the plasma permeability tensor without kinetic contribution. The perturbed electric field can be presented in the form $\mathbf{E} = (E_1, E_2, E_3)$, where

$$E_1 = \frac{\mathbf{k}_\perp \cdot \mathbf{E}}{k_\perp}, E_2 = \frac{\mathbf{k}_\perp \times \mathbf{E}}{k_\perp}, E_3 = \mathbf{b} \cdot \mathbf{E}, \mathbf{b} = \mathbf{B}/B, \tag{2}$$

where $\mathbf{B}$ is the equilibrium magnetic field. The polarization is given by the relation

$$E_1 = E_2 \frac{i\epsilon_2}{k_{\|}^2 - \epsilon_1}. \tag{3}$$

The parallel electric field of compressional Alfvén wave will be neglected.

To obtain the compressional Alfvén wave eigenmode equation we consider the perturbed parallel magnetic field in the form $\tilde{B}_{\|} = \tilde{B}_{\|}(r,\theta)\exp[-i(\omega t + n\varphi)]$, where θ and φ are the poloidal and toroidal angles, respectively, r is the minor radius of the magnetic surface. $\tilde{B}_{\|}$ is related to the perturbed electric field through the equation

$$\tilde{B}_{\|} = \frac{ck_{\perp}E_2}{\omega}. \tag{4}$$

The equlibrium magnetic field is chosen as $B = B_0R_0/(R_0 + r\cos\theta)$, where B_0 and R_0 are magnetic field and major radius at the plasma magnetic axis, respectively. Defining $k_{\|} = -i\mathbf{b}\cdot\nabla\ln\tilde{B}_{\|}$ we obtain the differential form of the dispersion relation as

$$[\nabla_r^2 + \frac{1}{r^2}\frac{\partial^2}{\partial\theta^2}]\tilde{B}_{\|} = -[\frac{\epsilon_2^2}{k_{\|}^2 - \epsilon_1} + \epsilon_1 - k_{\|}^2]\tilde{B}_{\|}, \tag{5}$$

where $\nabla_r^2 \equiv 1/r(\partial/\partial r)r(\partial/\partial r)$. For $\omega_{ci}^2 < \omega^2$ and $k_{\|}^2 < k_{\perp}^2$, Eq.(5) reduces to

$$[\nabla_r^2 + \frac{1}{r^2}\frac{\partial^2}{\partial\theta^2}]\tilde{B}_{\|} \simeq -\frac{\omega^2}{v_A^2}\tilde{B}_{\|}. \tag{6}$$

We will use Eq.(6) to study ACI eigenmode even for $\omega_{ci}^2 \sim \omega^2$. This equation has been studied in cylindrical plasma approximation.[9,13] In toroidal plasmas the eigenmode equation has been solved[8] in terms of an eikonal representation using the small parameters $1/m$ and $\epsilon = r/R_0$, where m is the poloidal mode number.

B. Radial eigenmode structure

In cylindrical plasma approximation the perturbed quantities can be presented in the form $\tilde{B}_{\|} = \hat{B}(r)\exp[-i\omega t - in\varphi + im\theta]$, where $\varphi = z/R$ and z is the coordinate along the plasma cylindrical axis. Then the eigenmode radial structure is described by the following

equation:

$$(\nabla_r^2 - V(r))\hat{B}(r) = 0, \tag{7}$$

where the potential is given by $V(r) \simeq m^2/r^2 - (\omega^2/v_A^2(0))(n(r)/n_0)$, $n(r)$ is the plasma density with the central density n_0, and $v_A^2(0)$ is evaluated at the magnetic axis with the vacuum toroidal magnetic field. If $V(r)$ forms a potential well, localized solutions can exist inside the well. For a plasma density profile of the form

$$n(r) = n_0(1 - r^2/a^2)^{\sigma_i}, \tag{8}$$

and if $m \gg 1$, a potential well can form at $r = r_0$, where $r_0^2/a^2 = 1/(1+\sigma_i) - \Delta^2/a^2$, and $\Delta^2/a^2 = \sqrt{2\sigma_i/(1+\sigma_i)}/[m(1+\sigma_i)]$. Then Eq.(7) can be approximated as a harmonic oscillator equation which admits localized solutions. The lowest most localized eigenmode solution has the eigenfrequency $\omega^2 = (m^2 v_A^2(r_0)/r_0^2)(1 + \sqrt{2(1+\sigma_i)/\sigma_i}/m)$ and

$$\hat{B}(r) = b\exp[-(r - r_0)^2/\Delta^2]. \tag{9}$$

Note that in the potential well region the solution (9) is consistent with the ordering

$$\frac{\partial \tilde{B}_{\|}}{\partial r} \sim \frac{\sqrt{m}\tilde{B}_{\|}}{r}, V(r) \sim \frac{m}{r^2}. \tag{10}$$

For $\sigma_i \leq 1$ the eigenmode is localized near the plasma edge. Thus, to form a potential well $V(r)$ near the plasma edge, it requires a rapid variation of the plasma density profile near the plasma periphery (see Fig.1).

To include the toroidal effects in the eigenmode equation, we note that $\omega^2/v_A^2 = (\omega^2/v_A^2(0))$ $(n(r)/n_0)(1+\epsilon\cos\theta)^2$. For high-m modes we consider $\partial^2\tilde{B}_{\|}/\partial\theta^2 \gg r^2\partial^2\tilde{B}_{\|}/\partial r^2$, which is satisfied by the cylindrical orderings, Eq.(10). Then, Eq.(6) reduces to

$$\frac{1}{r^2}\frac{\partial^2\tilde{B}_{\|}}{\partial\theta^2} = -\frac{\omega^2}{v_A^2(0)}\frac{n(r)}{n_0}(1+\epsilon\cos\theta)^2\tilde{B}_{\|}. \tag{11}$$

To the lowest order in (ϵ/m) Eq.(11) admits a solution in the form of

$$\tilde{B}_{\|} = \hat{B}(r,\theta)\exp[-i\omega t + iS], \tag{12}$$

where $S = -n\varphi + m(\theta + \epsilon\sin\theta)^8$ and $\hat{B}(r,\theta)$ is a slowly varying function of r and θ.

For $\epsilon \sim O(1/m)$ and considering the cylindrical ordering, Eq.(10), we have $\partial S/\partial r \ll \partial \ln \hat{B}/\partial r$. Substituting Eq.(12) into Eq.(6), we obtain an equation for the envelope $\hat{B}(r,\theta)$ which is identical to the cylindrical Eq.(7).

For larger ϵ we consider

$$\hat{B}(r,\theta) = \sum_l \hat{B}_l(r)e^{il\theta}, \tag{13}$$

and require $|l| \ll m$. From Eqs.(6),(13), and (12), we obtain the recurrence relation for the coefficients $\hat{B}_l(r)$

$$\left[\nabla_r^2 - V(r)(1+\frac{\epsilon^2}{2}) - \frac{l^2}{r^2} - \frac{2ml}{r^2} - \frac{m^2\epsilon^2}{2r^2}\right]\hat{B}_l = \epsilon^2[V(r) - \frac{m^2}{r^2}](\hat{B}_{l-2} + \hat{B}_{l+2})$$
$$+\epsilon\frac{m}{r^2}((l-1)\hat{B}_{l-1} + (l+1)\hat{B}_{l+1}) + \epsilon V(r)(\hat{B}_{l-1} + \hat{B}_{l+1}) - \epsilon\frac{m}{r}\frac{\partial}{\partial r}(\hat{B}_{l-1} - \hat{B}_{l+1}). \tag{14}$$

Assuming $\epsilon \sim O(1/m^{1/\nu})$ and $\nu > 2$ so that $m\epsilon^2 > 1$ and requiring the series, Eq.(13), to converge, $\hat{B}_l$ must be a decreasing function of $|l|$. For $l \sim O(1)$ the leading terms in Eq.(14) are proportional to $m^2\epsilon^2 \sim \epsilon^{-2(\nu-1)}$, and all $\hat{B}_l$ are of the same order. For larger l with $l > O(m\epsilon^2)$ we obtain $\hat{B}_l \simeq m\epsilon^2\hat{B}_{l-2}/2l$. Thus, $\hat{B}_l < \hat{B}_{l-2}$ and the series (13) converges. Therefore, the series (13) contains $\hat{B}_l$ with $l \leq m\epsilon^2$.

Since $l\theta \ll S$ the phase in $\hat{B}$ can be neglected. However, we need to calculate $\hat{B}_l$ from Eq.(14) for $l \leq m\epsilon^2$, which requires extensive numerical calculations. In the following we will approximate $\hat{B}$ with the cylindrical radial eigenmode given by Eq.(9).

C. Perturbative analysis

Using Eq.(4) the eigenmode equation, Eq. (5), can be rewritten in terms of the perturbed electric field and is given by

$$r\nabla_r^2/rE_2 = [\frac{1}{r^2}\frac{\partial^2}{\partial\theta^2} + k_\parallel^2 - \frac{\epsilon_2^2}{k_\parallel^2 - \epsilon_1} - \epsilon_1]E_2 \simeq V(r)E_2. \tag{15}$$

Considering resonance contributions to Eqn. (15) due to all plasma species to be small, we can make use of the perturbation method. We expand perturbed electric field and eigenfrequency as $E_2 = E_2^0 + \delta E_2$ and $\omega = \omega^0 + \delta\omega$, where δE_2 and $\delta\omega$ are small kinetic corrections to the MHD eigenmode and eigenfrequency solutions. These kinetic effects are described by the antihermitian part of the permeability tensor $\hat{\epsilon}_j^{A10}$ for each species j, which will be presented in Sec.III. Then, from Eq. (15) we have

$$\gamma \equiv Im(\delta\omega) \simeq -\sum_j Im\int E_2^*[-2i\hat{\epsilon}_{j12}^A\frac{\epsilon_2}{k_\parallel^2 - \epsilon_1} + \hat{\epsilon}_{j11}^A\frac{\epsilon_2^2}{(k_\parallel^2 - \epsilon_1)^2} + \hat{\epsilon}_{j22}^A]E_2 d^3r/$$
$$\int E_2^*[-\frac{2i}{\omega^2}\frac{\partial\omega^2\hat{\epsilon}_{12}}{\partial\omega}\frac{\epsilon_2}{k_\parallel^2 - \epsilon_1} + \frac{1}{\omega^2}\frac{\partial\omega^2\hat{\epsilon}_{11}}{\partial\omega}(1 + \frac{\epsilon_2^2}{(k_\parallel^2 - \epsilon_1)^2})]E_2 d^3r. \tag{16}$$

Taking into account Eq. (3) and neglecting parallel electric field, Eq. (16) can be rewritten as

$$\gamma = -\sum_j Im\int \mathbf{E}^*\cdot\hat{\epsilon}_j^A\cdot\mathbf{E}d^3r/\int \mathbf{E}^*\cdot\frac{1}{\omega^2}\frac{\partial\omega^2\hat{\epsilon}}{\partial\omega}\cdot\mathbf{E}d^3r \simeq$$
$$\simeq -\frac{\omega}{2}\sum_j Im\int E_1^*\hat{\epsilon}_{j11}^A E_1 d^3r/\int E_1^2 \mid \hat{\epsilon}_{11} \mid d^3r. \tag{17}$$

III. INTERACTION OF HIGH ENERGY PARTICLES WITH COMPRESSIONAL ALFVÉN WAVE

In this section we will use a WKB eikonal representation for perturbed quantities

$$\zeta \simeq \hat{\zeta}(\psi,\theta)e^{-i\omega+iS(s,\psi,\theta)},\ \nabla\zeta \simeq i\zeta\nabla S = i\zeta\mathbf{k}, \tag{18}$$

where ψ is the poloidal magnetic flux, the eikonal S will be chosen explicitly in Sec.IV, and s is the coordinate along the magnetic field so that $\mathbf{B}\cdot\nabla = B\partial/\partial s$. The perturbed vector and electrostatic potentials are chosen as

$$\mathbf{E} = -\nabla\phi + (i\omega/c)\mathbf{A}, \tilde{\mathbf{B}} = \nabla\times\mathbf{A}. \tag{19}$$

Then the fast particle contribution (subscripted as α) to the antihermitian part of the permeability tensor can be expressed through the resonance part of the perturbed distribution function:

$$\int \mathbf{E}^*\cdot\hat{\epsilon}^A_\alpha\cdot\mathbf{E}d^3r = \frac{4i\pi}{\omega}\int \mathbf{E}^*\cdot\tilde{\mathbf{j}}^A_\alpha d^3r = \frac{4i\pi}{\omega}e_\alpha\int \mathbf{E}^*\cdot\mathbf{v}_\alpha\tilde{f}^r_\alpha d^3v d^3r. \tag{20}$$

The perturbed fast particle distribution function can be expressed as (we delete the subscript α)

$$\tilde{f} = \frac{e}{m}\frac{\partial f}{\partial\mathcal{E}}\phi + \frac{e}{Bm}\frac{\partial f}{\partial\mu}\left(\phi - \frac{v_\parallel A_\parallel}{c}\right) + \frac{\mathbf{A}\times\mathbf{b}}{B}\cdot\nabla f$$
$$+\sum_{l=-\infty}^{+\infty}\left(g_l - \frac{e}{Bm}\frac{\partial f}{\partial\mu}\left[\left(\phi - \frac{v_\parallel A_\parallel}{c}\right)J_l - \frac{v_\perp\tilde{B}_\parallel}{ck_\perp}\frac{dJ_l}{dz}\right]\right)\exp(iL_l), \tag{21}$$

where f is the equilibrium distribution function, $J_l = J_l(z)$ is the $l-th$ order Bessel function of the first kind, $z = k_\perp v_\perp/\omega_c$, $\mu = v_\perp^2/2B$ is the magnetic momentum , $\mathcal{E} = v^2/2$ is the particle energy, $L_l = \mathbf{k}_\perp\times\mathbf{v}\cdot\mathbf{b}/\omega_c - l\beta$, β is the particle gyrophase angle between $\mathbf{v}_\perp$ and $\mathbf{k}_\perp$. The nonadiabatic part of the perturbed distribution function is contained in g_l, which is governed by the general frequency gyrokinetic equation[14-16]

$$(\omega - \omega_D - l\omega_c)g_l = \frac{ef}{T}(\tilde{\omega}_l - \omega_*^T)[(\phi - \frac{v_\parallel A_\parallel}{c})J_l - \frac{v_\perp\tilde{B}_\parallel}{ck_\perp}\frac{dJ_l}{dz}], \tag{22}$$

where

$$\omega_D = \frac{dS}{dt} = v_\parallel\mathbf{b}\cdot\nabla S + \omega_B m\mu B/T + \omega_k m v_\parallel^2/T,$$

$$\omega_B = cT/eB^2\ \mathbf{k}_\perp \cdot \mathbf{b} \times \nabla \mathbf{B},\ \omega_k = cT/eB\ \mathbf{k}_\perp \cdot \mathbf{b} \times \kappa_c,$$
$$\tilde{\omega}_l = -\frac{T}{m}(\omega\frac{\partial}{\partial \mathcal{E}} + \frac{l\omega_c}{B}\frac{\partial}{\partial \mu})\ln f,\ \omega_*^T = \frac{cT}{eB}\mathbf{k}_\perp \cdot \mathbf{b} \times \nabla \ln f, \tag{23}$$

κ_c is the magnetic field curvature, and T is the temperature of given species. Equation (22) can be rewritten in the form

$$(\frac{d}{dt} + il\omega_c)g_l = -iX. \tag{24}$$

where X is the rhs of Eq. (22). We integrate Eq. (23) along the particle characteristics[10] with the casuality condition that at $t' = -\infty$, g_l vanishes, and obtain

$$g_l(t) = -i\int_{-\infty}^{t} dt'\hat{X}'\exp\left(-i\omega t' + iS(s',\psi',\theta') + i\int_t^{t'} l\omega_c dt''\right), \tag{25}$$

where the integral is taken along the unperturbed guiding-center trajectory. Let

$$W(t) \equiv \int_0^t (\omega_D - \bar{\omega}_D + l\omega_c - l\bar{\omega}_c)dt' \tag{26}$$

with $\overline{(...)} = \oint dt(...)/\tau_b$ taken along the particle orbit, $\tau_b = 2\pi/\mid \omega_b \mid$ and $\omega_b = 2\pi[\oint \frac{ds}{v_\parallel}]^{-1}$. Then

$$\hat{g}_l(t) = -i\int_{-\infty}^{t} dt'\hat{X}'\exp\left[iW(t') - iW(t) - i(\omega - \bar{\omega}_D - l\bar{\omega}_c)(t'-t)\right]. \tag{27}$$

Note that $\hat{X}'\exp[iW(t')]$ is periodic in time with the bounce period and can be decomposed[17] as:

$$\hat{X}'\exp\left(iW(t')\right) = \sum_p \hat{X}_p \exp\left(ip\omega_b t'\right), \tag{28}$$

where $\hat{X}_p = \overline{\hat{X}\exp\left(iW(t) - ip\omega_b t\right)}$.

For the nonadiabatic part of the perturbed current [see Eq. (20)] we have after gyrophase averaging

$$\tilde{\mathbf{j}}^A = e\sum_l \int v_\perp dv_\perp dv_\parallel \mathbf{G}_l'^* g_l, \tag{29}$$

where the components of the vector $\mathbf{G}_l'$ are $v_\perp l J_l(z)/z$, $iv_\perp \partial J_l/\partial z$ and $v_\parallel J_l$. Substituting Eq. (29) into Eq. (20) and integrating Eq. (27) we have

$$\int \mathbf{E}^* \cdot \hat{\epsilon}^A \cdot \mathbf{E} d^3r = \frac{4i\pi e}{\omega} \sum_{l,p} \int d^3r v_\perp dv_\perp dv_\parallel \frac{\mathbf{E}^* \cdot \mathbf{G}_l'^* \exp(-iW(t) + ip\omega_b t)\hat{X}_p}{\omega - l\bar{\omega}_c - \bar{\omega}_D - p\omega_b}. \tag{30}$$

To make this equation more symmetric we express

$$\phi - \frac{v_\parallel A_\parallel}{c} \simeq i\frac{E_1}{k_\perp} + i\frac{v_\parallel E_3}{\omega}, \tag{31}$$

where $k_\parallel/k_\perp \ll 1$ is assumed. Then we have

$$\hat{X}_p = \frac{ief}{\omega T}(\tilde{\omega}_l - \omega_*^T)F_{lp}, \tag{32}$$

where $F_{lp} = \overline{\exp(iW(t) - ip\omega_b t)\mathbf{G}_l \cdot \hat{\mathbf{E}}}$ and $\mathbf{G}_l = \{v_\perp \omega J_l(z)/(\omega_c z); iv_\perp \partial J_l/\partial z; v_\parallel J_l\}$. Here the equilibrium distribution function is assumed to be a function of the particle's integrals of motion. Returning to Eq. (30) we note that the integration is taken over five-dimensional phase space. We will extract the fast integration along the unperturbed particle trajectory associated with the variable t in Eq. (30). We transform integration variables from $R, Z, \varphi, v_\perp, v_\parallel$ to $P_\varphi, \psi, \varphi, \mu, \mathcal{E}$, where

$$P_\varphi = \frac{e\psi(R,Z)}{2\pi\, mc} - v_\varphi R \tag{33}$$

is the longitudinal adiabatic invariant. Then we have

$$v_\perp R dR dZ d\varphi dv_\perp dv_\parallel = [\frac{\partial\psi}{\partial Z}\frac{\mathcal{E}}{\omega_c R}(1 + \frac{v_\parallel^2}{v^2})]^{-1}\frac{B}{\omega_c} d\psi dP_\varphi d\varphi d\mu d\mathcal{E}, \tag{34}$$

where we assumed $v_\parallel \simeq v_\varphi$. The particle orbit motion is associated with the variable ψ, so that $dt = [\frac{\partial\psi}{\partial Z}\frac{\mathcal{E}}{\omega_c R}(1 + \frac{v_\parallel^2}{v^2})]^{-1} d\psi$. Thus, taking into account Eqs. (32) and (34) and Eq. (30) we result in

$$\int \mathbf{E}^* \cdot \hat{\epsilon}^A \cdot \mathbf{E} d^3r = -\frac{8\pi^2 e^2 B}{\omega_c \omega^2 T} \int dP_\varphi d\mu d\mathcal{E} f \tau_b \sum_{l,p} \frac{F_{lp}'^*(\tilde{\omega}_l - \omega_*^T)F_{lp}}{\omega - l\bar{\omega}_c - \bar{\omega}_D - p\omega_b}, \tag{35}$$

where $F'_{lp} = \overline{\exp(iW(t) - ip\omega_b t)\mathbf{G}'_l \cdot \hat{\mathbf{E}}}$. A similar expression was analyzed in[10] in the limit of zero banana width and with F_{lp} computed for well trapped and passing particles.

The p summation can be performed in a general form. First, the resonance term is expanded as

$$R^{-1}(P_\varphi, \mu, \mathcal{E}) \equiv (\omega - l\bar{\omega}_c - \bar{\omega}_D - p\omega_b)^{-1} = \frac{\mathcal{P}}{\omega - l\bar{\omega}_c - \bar{\omega}_D - p\omega_b} - i\pi\delta(R). \tag{36}$$

Retaining only the resonance contribution Eq. (35) is integrated over μ. Then we make the following approximation

$$\sum_p \rightarrow \int dp \rightarrow \int \frac{\partial p}{\partial \mu} d\mu, \tag{37}$$

where p is considered as a function of μ and is determined by $p(\mu) = (\omega - l\bar{\omega}_c - \bar{\omega}_D)/\omega_b$. The approximation (37) is reasonable if $\mu\partial p/\partial\mu \gg 1$, which is valid because we consider high frequency modes with $\omega \simeq \omega_c \gg \omega_b$. Finally employing Eq. (37) and bearing in mind that $\mid \partial p/\partial\mu \mid / \mid \partial R/\partial\mu \mid = 1/\mid \omega_b \mid$ we obtain:

$$\int \mathbf{E}^* \cdot \hat{\epsilon}^A \cdot \mathbf{E} d^3r = i\sum_l \frac{4\pi^2 e^2 B}{\omega_c \omega^2} \int dP_\varphi d\mathcal{E} d\mu \frac{f\tau_b^2}{T} F_l'^*(\tilde{\omega}_l - \omega_*^T) F_l, \tag{38}$$

where we have made use of the bounce resonance conditions and the definition

$$\begin{aligned} F_{lp} &= \frac{1}{\tau_b} \oint dt \exp(iW(t) - ip(\mu)\omega_b t)\mathbf{G}_l \cdot \mathbf{E} = \\ &= \frac{1}{\tau_b} \oint dt \exp(i\int_0^t (l\omega_c + \omega_D - \omega)dt')\mathbf{G}_l \cdot \mathbf{E} \equiv F_l. \end{aligned} \tag{39}$$

The expression (38) is still too complicated for analytical analysis. To further simplify F_l we note that the argument in the exponential function is much larger than π, which means that the exponential function is fast oscillating except near the region where $l\omega_c(\theta(t_1)) + \omega_D(\theta(t_1)) - \omega = 0$, where $\theta(t_1)$ is the poloidal angle of the particle position on the orbit at

time t_1. Around this point we have

$$i\int_{t_0}^{t}[l\omega_c+\omega_D-\omega]dt' = i\int_{t_0}^{t_1}[\ldots]dt' + i\int_{t_1}^{t}[\ldots]dt' = i\alpha_{01} + i\int_{t_1}^{t}[\ldots]dt', \tag{40}$$

where

$$i\int_{t_1}^{t}[\ldots]dt' = i\frac{d}{dt}(l\omega_c+\omega_D)\frac{(t-t_1)^2}{2} + i\frac{d^2}{dt^2}(l\omega_c+\omega_D)\frac{(t-t_1)^3}{6} + \ldots, \tag{41}$$

$\alpha_{ij} = \int_{t_i}^{t_j}[l\omega_c+\omega_D-\omega]dt'$, and t_0 corresponds to the radially outer most point of the particle orbit. The same expansion is valid for any resonant point. With a given set of variables $P_\varphi, \mathcal{E}, \mu$ there are two types of particle orbits which correspond to different sign of parallel velocity $\sigma = v_\parallel/v$. Assuming up-down symmetric particle orbits there can be two resonance points at poloidal angles θ_{res} and $-\theta_{res}$ determined by the resonance condition $l\omega_c(\theta_{res}) + \omega_D(\theta_{res}) - \omega = 0$ for each σ. We will show the calculation procedure for the case when the first derivative term in Eq. (40) is larger than the second derivative term. For trapped particles there may be four resonance points. Then we have

$$F_l = \frac{1}{\tau_b}\mathbf{G}_1\cdot\mathbf{E}_1 e^{i\alpha_{01}}\left(I_1 + \frac{\mathbf{G}_2\cdot\mathbf{E}_2}{\mathbf{G}_1\cdot\mathbf{E}_1}e^{i\alpha_{12}}I_1^*\right) + \frac{1}{\tau_b}\mathbf{G}_3\cdot\mathbf{E}_3 e^{i\alpha_{03}}\left(I_3 + \frac{\mathbf{G}_4\cdot\mathbf{E}_4}{\mathbf{G}_3\cdot\mathbf{E}_3}e^{i\alpha_{34}}I_3^*\right), \tag{42}$$

where we denote the resonance points $1,3$ in the upper half cross section for $\sigma = +1, -1$, respectively, and the points 2,4 in the lower half cross section for $\sigma = +1, -1$, respectively. Also, $I_{1,3} = \int_{-\infty}^{+\infty}\exp[i(d(l\omega_c+\omega_D)/dt)_{1,3}t^2/2]dt$. Then we can write

$$F_l'^* F_l = \frac{I_1^2}{2\tau_b^2}\sum_{i=1,2}\mathbf{G}_i'^*\cdot\mathbf{E}_i^*\mathbf{G}_i\cdot\mathbf{E}_i + \frac{I_3^2}{2\tau_b^2}\sum_{i=3,4}\mathbf{G}_i'^*\cdot\mathbf{E}_i^*\mathbf{G}_i\cdot\mathbf{E}_i, \tag{43}$$

where we have dropped terms with $e^{i(\alpha_{ij}+\alpha_{kl})}, i\neq k, j\neq l$, which correspond to uncorrelated phase and give zero contribution after averaging over all groups of particles, and obtained

$$I_{1,3}^2 = 8\pi/\left|\frac{d}{dt}(l\omega_c+\omega_D)\right|_{1,3}. \tag{44}$$

Similar expression can be obtained for untrapped particles, with the first term in Eq. (43) for passing particles with $\sigma = 1$ and the second term for $\sigma = -1$. Summing over the parallel velocity direction σ, we arrive at the following expressions:

$$F_l'^* F_l = (2\tau_b)^{-2} \sum_\sigma I^2 \left(\mathbf{G}'^* \cdot \mathbf{E}^* \mathbf{G} \cdot \mathbf{E}_{|\theta_{res}} + \mathbf{G}'^* \cdot \mathbf{E}^* \mathbf{G} \cdot \mathbf{E}_{|-\theta_{res}} \right), \tag{45}$$

where

$$I^2 = \frac{8\pi}{\{| \, d(l\omega_c + \omega_D)/dt \, |^3 + C[d^2(l\omega_c + \omega_D)/dt^2]^2\}^{1/3}} \tag{46}$$

with the subscripts dropped, and $C = 2.6943$. Also, to avoid singularity at $\theta_{res} = 0$ the next order term from the expansion (40) is included. The coefficients $F_l'^* F_l$ determined by Eq. (45) contain the information about the wave-particle Doppler shifted cyclotron resonance. Namely, the two terms in the round brackets gives the electric field value at the resonance point and the factors $\mathbf{G}'$ and $\mathbf{G}$ appear from gyroaveraging. The term I has the dimension of time and determines how long the particle was in a resonant layer.

In summary, the ACI growth rate due to fast particles is given by Eq. (17) with the antihermitian tensor given by Eqs. (38) and (45). These expressions take into account the high frequency wave-particle resonance in phase space along the particle orbit.

IV. ALFVÉN CYCLOTRON INSTABILITY

A. Fast particle destabilization

In this section we demonstrate the possibility that ACI in tokamak plasmas can be excited by a small group of high energy particles (α-particles or protons). From Eq. (3), E_2 is smaller than E_1 for $\omega > \omega_c$ and can be ignored. Thus the perturbed electric field can be expressed

in the form $\mathbf{E} \simeq E_1, 0, 0$, where

$$E_1 = E_0 \exp[-(r - r_0)^2/\Delta^2] \exp[-i\omega t - in\varphi + im(\theta + \epsilon \sin\theta)], \tag{47}$$

and r_0 and Δ are given in Eq. (9). Then $k_{\|} = m/qR_0 - n/R, k_{\perp} \simeq mR/rR_0$. For $S = -n\varphi + m(\theta + \epsilon \sin\theta)$ the magnetic drift frequency $\omega_{D\alpha}$ defined in Eq. (23) is given by

$$\begin{aligned} \omega_{D\alpha} &= (mR/R_0 - nq)\dot{\theta} - n\mathbf{v}_{d\alpha}(\nabla\varphi - q\nabla\theta) \\ &\simeq k_{\|}\sqrt{2\mathcal{E}}\sqrt{1 - \mu B/\mathcal{E}} + \frac{2nq}{r^2}\frac{\mathcal{E}}{\omega_{c\alpha 0}}\left(\frac{R}{R_0} - 1\right)\left(1 - \frac{\mu B}{2\mathcal{E}}\right). \end{aligned} \tag{48}$$

The fast particle driven growth rate can be obtained from Eqs. (17), (38), and (45) by neglecting the spatial gradient drive term, which is negligible in the high frequency regime, and is given by

$$\frac{\gamma_\alpha}{\omega_{c\alpha}} = \frac{\omega^3}{\omega_p^2\omega_{c\alpha}^2}\frac{\sqrt{2}e_\alpha cB}{\sqrt{\pi}\Delta r_0 R_0 E_0^2}\sum_{l,\sigma}\int dP_\varphi d\mathcal{E} d\mu I^2 E_1^2 \frac{\mu l J_l^2}{z^2}\left[\frac{\partial}{\partial\mathcal{E}} + \frac{l\omega_{c\alpha}}{\omega B}\frac{\partial}{\partial\mu}\right] f_\alpha, \tag{49}$$

where we assumed for simplisity that $\hat{\epsilon}_{11} \simeq \omega_p^2/\omega^2$ and ω_p is the plasma frequency. The sign of the growth rate depends on the $\mathcal{E}$ and μ derivatives of the distribution function. We mentioned earlier that the plasma inhomogeneity and finite banana width can lead to large velocity space anisotropy of α-particle distribution. The anisotropy is higher near the plasma periphery, where the spatial gradient of α-particle source is higher.[12] A limiting case of the distribution function, a delta function in μ which represents only the contribution of the barely trapped particles, is considered. The orbits of the barely trapped particles are shown by curves 1 and 2 in Fig.2. Such a group of particles have the maximum orbit deviation from the magnetic surface and their fusion source is maximum in comparison with other groups. The α-particle distribution can be expressed as

$$f_\alpha = n_\alpha(r) f_v(v)\delta\left(\frac{\mu B_0}{\mathcal{E}} - \Lambda_0\right), \tag{50}$$

where $f_v(v)$ represents the velocity distribution, and Λ_0 is the pitch angle of barely trapped particles. Λ_0 can be obtained from the equation $(e_\alpha/2\pi m_\alpha c)\psi(R,Z)_{|R=\Lambda_0 R_0, Z=0} = P_\varphi$ (compare with Eq.(33)). Integrating by parts with the distribution (50), Eq. (49) reduces to

$$\frac{\gamma_\alpha}{\omega_{c\alpha}} = \frac{\omega^3}{\omega_p^2\omega_{c\alpha}^2}\frac{\sqrt{2}e_\alpha cB}{\sqrt{\pi}\Delta r_0 R_0 E_0^2}\sum_{l,\sigma}\int dP_\varphi \times$$
$$\times\left\{F(\mathcal{E}_2) - F(\mathcal{E}_1) - \int d\mathcal{E} n_\alpha f_v \frac{\mathcal{E}}{B_0}\left[\frac{\partial}{\partial\mathcal{E}} + \frac{l\omega_{c\alpha}}{\omega B}\frac{\partial}{\partial\mu}\right] I^2 E_1^2 \frac{\mu l J_l^2}{z^2}\right\}_{|\mu=\Lambda_0\mathcal{E}/B_0}, \tag{51}$$

where $F = (1 + l\omega_{c\alpha}\mathcal{E}/(\omega B\mu))n_\alpha f_v \frac{\mathcal{E}}{B_0} I^2 E_1^2 \mu l J_l^2/z^2$, $\mathcal{E}_{1,2} = \mathcal{E}_{1,2}(P_\varphi)$ $(\mathcal{E}_1 < \mathcal{E}_2)$ are the energy limits determined from resonance condition at fixed P_φ. The differential operators in Eq. (51) operate on all quantities to their right hand side. These quantities are taken at resonance point and therefore are functions of P_φ and $\mathcal{E}$. The resonance condition is

$$\omega - l\omega_{c\alpha}(r(\theta),\theta) - \omega_D(r(\theta),\theta) = 0, \tag{52}$$

where $r(\theta)$ determines the α-particle orbit. In comparison with the local theory[8,9] Eq. (51) have additional terms proportional to derivatives of I^2 and E_1^2. One can show that the I^2 derivative terms give small contribution, while the E_1^2 derivative terms are always destabilizing and are comparable with the $\mu J_l^2/z^2$ derivative terms from the local theory. Note that the α-particle growth rate is linear in α-particle density.

B. Damping mechanisms and ICE spectrum

To excite the ACI the fast ion drive must be higher than all dampings due to thermal electrons and ions. To obtain the most unstable modes we have to find a condition when the damping is smallest and the drive is largest. To minimize the electron damping we choose the eigenmodes with the wave phase velocity higher than the thermal velocity of electrons,[8,11] i.e., $k_\parallel \ll \omega/v_{Te}$, so that the electron damping is exponentially small. Ion cyclotron damping

can be significant if ions are in cyclotron resonance with the wave at $l = \omega/\omega_{ci} < 5$ inside the plasma core. Therefore, eigenmodes localized near the plasma edge and with frequency corresponding to edge background ion cyclotron frequencies can be weakly damped due to low ion density. For higher cyclotron harmonics with $l = \omega/\omega_{ci} > 5$ the thermal ion damping is exponentially small. The accurate calculation of thermal plasma damping mechanisms is beyond the scope of this paper.

For simplicity we will present the growth rate calculation for the ACI eigenmodes with negligible thermal plasma damping and with eigenfrequencies corresponding to the multiples of deuterium (α- particle) cyclotron frequency. Such ICE spectrum was experimentally observed in DD experiments and in the initial stage of DT experiments in TFTR when the tritium population is small. We will show that the fast particles can destabilize the ACI even when the ACI eigenfrequencies are different from the fast particle cyclotron frequency. They can be in cyclotron resonance due to the finite Doppler shift in the resonance condition (52). For example fast protons can drive ACI with frequencies $\omega = \omega_{cD}(2l+1) = \omega_{cp}(l+1/2)$. The ICE spectrum peaks can be also related to the tritium cyclotron frequencies. The results could be useful in estimating the ratio of tritium to deuterium densities.

C. Numerical results

We present numerical examples of ACI growth rates for TFTR plasma parameters[18]: $R_0 = 2.52m$, $a = 0.9m$, the safety factor profile is given by $q(r) = q_0/[\frac{d}{d(r^2)}(1 - 0.66r^2/a^2 + .18r^4/a^4)r^2]$ for $r \leq a$ and is a parabolic outside the plasma, $q_0 = 0.85$, the plasma density is $n(r) = 0.5 \times 10^{14}(1 - r^2/a^2)^{0.2} cm^{-3}$, the vacuum toroidal magnetic field is $B_0 = 5T$, the central α-particle density is $n_{\alpha 0} = 2 \times 10^{10} cm^{-3}$, the central proton density is $n_{p0} = n_{\alpha 0}/50$, and the fast particle density profile is $n_{\alpha,p} = n_{\alpha,p0}(1 - r^2/a^2)^{3.75}$. The position of the plasma

column in the vacuum vessel is shown on Fig. 2 as dotted circle.

In order to excite the ACI instabilities it is required for the eigenmodes to be localized in a potential well very close to the plasma periphery. This can be achieved by employing a density profile with very sharp variation near the plasma edge (see Fig.1). Choosing the parameter $\sigma_i = 0.2$ so that $r_0 \simeq 0.9a$. The plasma with such sharp density variation near the plasma edge can be obtained in the initial stage of typically TFTR discharges.[18] The frequencies of the ACI eigenmodes are assumed to be equal to multiples of the edge deuterium cyclotron frequency. The poloidal mode number m is calculated from the expression for eigenfrequency (Sec. B). The toroidal mode number is varied to find the most unstable mode with the constraint $k_{\|} \ll k_{\perp}$. Due to the finite Doppler shift from the magnetic drift frequency in the cyclotron resonance, Eqs. (48) and (52), α-particles will resonate with the wave inside the plasma while thermal ions can be in cyclotron resonance near the plasma edge. The dashed curve between point 1 and 2 in Fig.2 presents the resonance line for the barely trapped α-particles at the fundamental Doppler shifted cyclotron resonance.

The α-particle driven ACI growth rates are shown in Figs.3 (a) and (b) and the protons driven ACI growth rates are shown in Figs.4 (a) and (b) with a velocity distribution in the form:

$$f_v = \frac{4B_0}{Bv_0^2(v_{T-} + v_{T+})\sqrt{\pi}}\sqrt{1 - \Lambda_0\frac{B}{B_0}}\sum_{+,-}\exp\left(-\frac{(v - v_0)^2}{v_{T\pm}^2}\right)\eta(\pm(v - v_0)), \qquad (53)$$

where v_{T-} is an adjustable parameter, $v_{T+} = \sqrt{2T_i/(m_1 + m_2)}$, m_1 and m_2 are the masses of reacting nuclei, T_i is their temperature which was assumed to be $50keV$ for beam heated plasma, and η is the Heviside step function. Note that the parameter v_{T-} is critical for the ACI instability. For α-particles the instability disappears at $v_{T-} > 0.25v_{\alpha 0}$, while for protons the instability occurs at $v_{T-} > 0.8v_{\alpha 0}$. The slowing-down distribution is stable due to high

fast particle Landau damping. The destabilization from the velocity anisotropy term is not enough for instability. To drive ACI unstable one needs additional drive due to positive energy gradient. We note that the distribution given in Eq. (53) can be created at the initial stage of discharge after the fast NBI starts. The velocity spread is due to the Doppler shift effect associated with the velocity spread of the thermal fusion ions. The velocity distribution (53) can also be a result of anomalous fast particle loss caused by toroidal magnetic field ripples, or plasma instabilities such as the TAE, the fishbone, or other MHD modes. As a result of such losses the fast particle confinement time can be shorter than the slowing-down time, and the velocity distribution can maintain a positive gradient. An experimental evidence has been pointed out in[3] that the Edge Localized Modes (ELM) activity and the ICE amplitude are correlated; small amplitude ELMs do not disturb the ICE spectrum, while high amplitude ELMs can eliminate ICE completely. This related to the anomalous fast particle loss by ELM activities. Small ELM amplitude only reduces the fast ion confinement time to less than the slowing down time. High amplitude ELMs scatter almost all trapped fast particles out off the plasma. After the trapped particle population replenishes near the edge, the ICE appears again.

The α-particle birth velocity is different from the proton's: $v_A \sim v_{\alpha 0} \simeq 1.3 \times 10^9 cm/sec < v_{p0} \simeq 2.4 \times 10^9 cm/sec$. From Fig. 3($a$) one can see that the instability disappears for $l > 6$ because of a decrease in the destabilizing contribution associated with the spatial derivative of E_1^2. This term is destabilizing because of two reasons. The first reason is that the region with positive derivative of E_1^2 is closer to the center than the region with negative slope of eigenfunction, the second is that the α-particle density profile is centrally peaked. For higher cyclotron harmonics the region where particles are in resonance with the wave is smaller and the corresponding curve of resonance points (curve 1-2 in Fig.2)

moves out towards the plasma edge. Therefore, the positive spatial derivative of E_1^2 gives smaller destabilizing contribution to ACI. For protons the Doppler shift is higher and the reduction of the resonance domain does not lead to such effects. In addition, the value $z = k_\perp v_\perp/(l\omega_c)(\sim 2)$ is higher, which makes the local contribution to ACI ($\sim \mu J_l^2/z^2$) more destabilizing.

From Figs. 3(a) and 4 (a) we see that the proton growth rates are about one order smaller than the α-particle growth rate. We expect that in TFTR experiments both kinds of particles contribute to the ACI instability. In Figs.4 ((a)) and ((b)) we show the growth rate of the proton driven ACI at $\omega = \omega_{cD} = 1/2\omega_{cp}$ as a dashed bar. This instability can be obtained only at $k_\parallel \sim k_\perp$, which is beyond the validity of our assumptions. But, we should also note that the electron damping will be small in this case because of small wave phase velocity and $v_e \gg v_A$. Only trapped electrons with velocity $v_{e\parallel} \sim v_A$ can give rise to the damping, which requires additional analysis.

V. CONCLUSIONS

A two-dimensional theory of compressional Alfvén Cyclotron Instability has been developed to describe the ICE spectrum observed in TFTR and JET experiments. The final expression for the ACI growth rate Eq.(38) is determined by the Doppler shifted wave-particle cyclotron resonance. The source of instability can be any free energy source associated with fast particle distribution function, namely spatially or velocity space gradients. The expressions for ACI growth rates were used in numerical calculations in a toroidal plasma with circular magnetic surfaces. Fast particle resonance contributions resulting from the two-dimensional eigenmode structure and finite banana width effects are retained. We have

demonstrated that the theory can describe the narrow peaks at multiples of edge deuterium cyclotron frequency. The theory requires the ACI eigenmode to be localized near the very edge of plasma and the velocity distribution function to be very narrow in pitch angle and sufficiently sharp in velocity gradient with velocity spread for α-particles less than $0.25v_{\alpha 0}$, while for protons less than $0.8v_{\alpha 0}$. The velocity spread can be understood by taking into account the Doppler shift effect due to thermal spread of the fusion source ions. Such a distribution can exist if fast particles are lost before they are slowed down. Such anomalous loss of fast particles can result from toroidal magnetic field ripple, collisional scattering, or MHD activity like fishbone, TAE modes or Edge Localized Modes. The correlation between the ELM activities and the ICE amplitude has been shown in[3]; the small amplitude ELMs do not disturb the ICE spectrum, while high amplitude ELMs can eliminate the ICE completely. This is because small amplitude ELMs reduce only the confinement time to less than the slowing down time, while high amplitude ELMs scatter almost all trapped fast particles out of the plasma. After the population of trapped particles replenishes near the edge the ICE appears again. Note that in the eigenmode analysis we have excluded the region between the plasma current channel and the wall. In this region the eigenmode has a finite amplitude and the wave-particle interaction can contribute to stability and should be included. We have obtained the growth rates only for eigenmodes with frequencies equal exactly to multiples of the edge deuterium cyclotron frequency. But one also expects that the widths of higher harmonic ICE spectral peaks should be wider than those of lower cyclotron harmonic cases because the Doppler shift for protons is larger and the background ion cyclotron damping is smaller for higher cyclotron harmonics. Such wider peaks can form the background proton driven signal which should correlate with fusion proton source. This conclusion agrees well with the observed spectra.[1,2] We have also shown that the ACI with eigenfrequency differ-

ent from the cyclotron frequency of the fast particles can be driven unstable because the cyclotron resonance condition (52) can still be satisfied due to the finite Doppler shift. For example, protons can destabilize the ACI with frequencies $\omega = \omega_{ci}(2l + 1) = \omega_{cp}(l + 1/2)$, which may be also related to the ICE spectrum peaks at tritium frequencies. This conclusion can be useful in estimating the ratio of tritium to deuterium densities.

VI. ACKNOWLEDGMENTS

This work was supported by the United States Department of Energy under Contract No. DE-AC02-CHO-3073. One of us (N. N. G.) was supported partially under the Personnel Exchange II,10 of the US/RF Collaborative Program. We would like to thank Drs. C. S. Chang, R. Majeski, S. Cauffman, S. J. Zweben and R. O. Dendy for helpful discussions.

References

[1]G. J. Greene and the TFTR Group, in *Proceedings of 17th European Conference on Controlled Fusion and Plasma Heating*, Amsterdam, Netherlands, 1990, edited by G. Briffod, Adri Nijsen-Vis, and F. C. Shüller (European Physical Society, Petit-Lancy, Switzerland, 1990), Part IV, Vol. 14B, p.1540.

[2]R. Majeski and S. Cauffman, private communication.

[3]G. A. Cottrell, V. P. Bhatnagar, O. Da Costa, *et. al.*, Nucl. Fusion **33**, 1365 (1993).

[4]G. A. Cottrell and R. O. Dendy, Phys. Rev. Lett. **60**, 33 (1988).

[5]R. O. Dendy, C. N. Lashmore-Davies, and K. F. Kam, Phys. Fluids B **4**, 3996 (1992).

[6]R. O. Dendy, C. N. Lashmore-Davies, and K. F. Kam, Phys. Fluids B **5**, 1937 (1993).

[7]V. S. Belikov, Ya. I. Kolesnichenko, IAEA α-particle Technical Committee Meeting, Trieste, Italy, 1993, to be published in Fusion Technology.

[8]B. Coppi, S. Cowley, R. Kulsrud, P. Detragiache, F. Pegoraro, Phys. Fluids **29**, 4060 (1986).

[9]B. Coppi, Physics Letters A **172**, 439 (1993).

[10]A. B. Mikhailovskii, in *Reviews of Plasma Physycs*, edited by M. A. Leontovich (Consultants Bureau, New York, 1986), Vol. 9, p.103.

[11]A. I. Akhiezer et. al., Plasma Electrodinamics (Pergamon Press, Oxford, New York, 1975), Vol. 1.

[12]N. N. Gorelenkov, Sov. J. Plasma Phys. **18**, 289 (1992).

[13]S. M. Mahajan, D. W. Ross, Phys. Fluids **26**, 2561 (1983).

[14]L. Chen, S. T. Tsai, Plasma Phys. **25**, 349 (1983).

[15]X. S. Lee, J. R. Myra, P. J. Catto, Phys. Fluids **26**, 223 (1983).

[16]H. L. Berk, C. Z. Cheng, M. N. Rosenbluth, and J. W. Van Dam, Phys. Fluids **26**, 2642 (1983).

[17]C. Z. Cheng, Phys. Fluids B **3**, 2463 (1991).

[18]R. V. Budny et al., Nucl. Fusion **32**, 429 (1992).

Figure 1: Typical radial dependence of the potential $V(r) = \omega^2/v_A^2 - m^2/r^2$ on r^2/a^2, which forms a well at $r = r_0$ and r_0 is determined in Eq. (9) The eigenmode is localized within the 2Δ width region.

Figure 2: Wall position, plasma boundary (dotted line) and two orbits of barely trapped particles with different pitch angle. Also shown is the resonance curve (dashed curve) between resonance points 1 and 2 at which the resonance condition (52) is fulfilled

Figure 3: The ACI growth rates driven by α-particles with the velocity distribution, given by Eq.(53) for $a)$ $v_{T-} = v_{T+} = 0.107 v_{\alpha 0}$ and $b)$ $v_{T-} = 0.2 v_{\alpha 0}, v_{T+} = 0.107 v_{\alpha 0}$. The plasma parameters are: $B_0 = 5T$, $R_0 = 2.52m$, $a = 0.9m$, the plasma density is $n(r) = 0.5 \times 10^{14}(1 - r^2/a^2)^{0.2} cm^{-3}$, $q(r) = q_0/[\frac{d}{d(r^2)}(1 - 0.66r^2/a^2 + .18r^4/a^4)r^2]$, for $r \leq a$ and is a parabolic outside the plasma, $q_0 = 0.85$, and the α-particle density is $n_\alpha(r) = 2 \times 10^{10}(1 - r^2/a^2)^{3.75} cm^{-3}$.

Figure 4: The ACI growth rates driven by protons with the velocity distribution, given by Eq.(53) and $a)$ $v_{T-} = v_{T+} = 0.058 v_{p0}$ and $b)$ $v_{T-} = 0.55 v_{p0}, v_{T+} = 0.058 v_{p0}$. The first dashed bar at $\omega/\omega_{cDedge} = 1$ corresponds to the case when $k_{\|} \sim k_{\perp}$. The proton density is chosen as $n_p(r) = 0.4 \times 10^9(1 - r^2/a^2)^{3.75} cm^{-3}$. The plasma parameters are the same as in Fig.3.

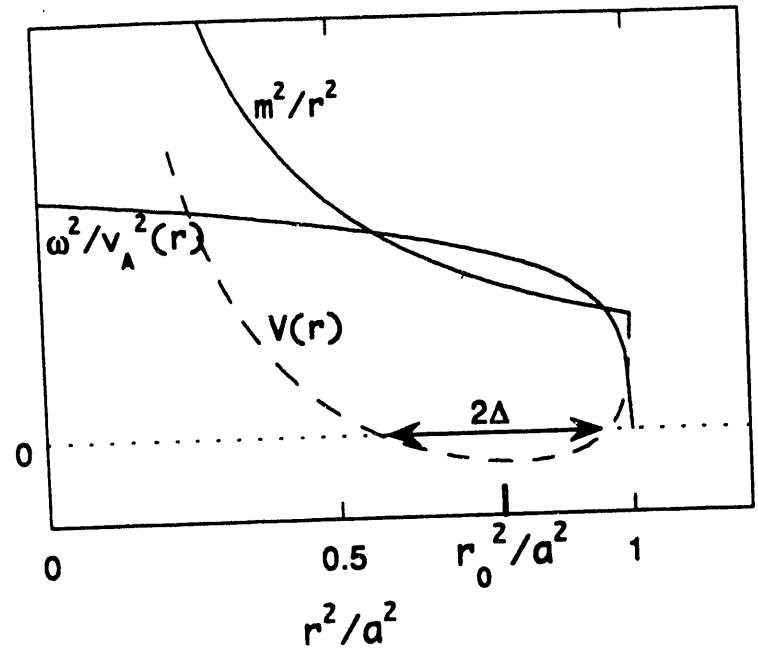
m²/r²
ω²/v_A²(r)
V(r)
2Δ
0
0
0.5
r₀²/a²
1
r²/a²

Fig.1

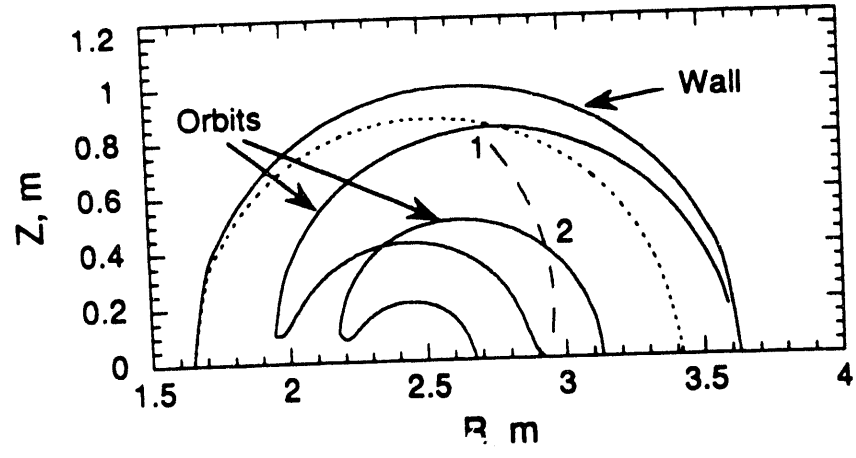
Wall
Orbits
1
2
Z, m
R m
1.2
1
0.8
0.6
0.4
0.2
0
1.5
2
2.5
3
3.5
4

Fig.2.

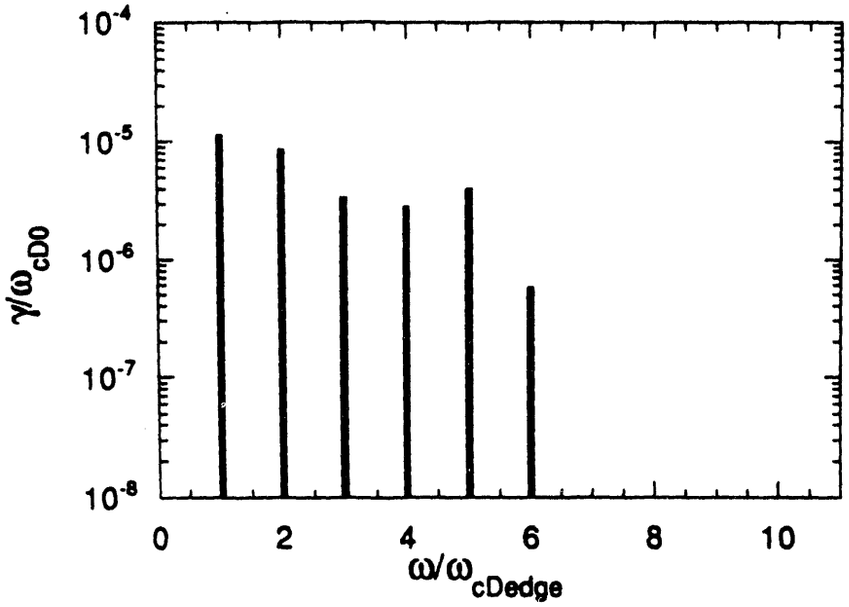
10-4
10-5
10-6
10-7
10-8
γ/ωcD0
0
2
4
6
8
10
ω/ωcDedge

Fig.3a.

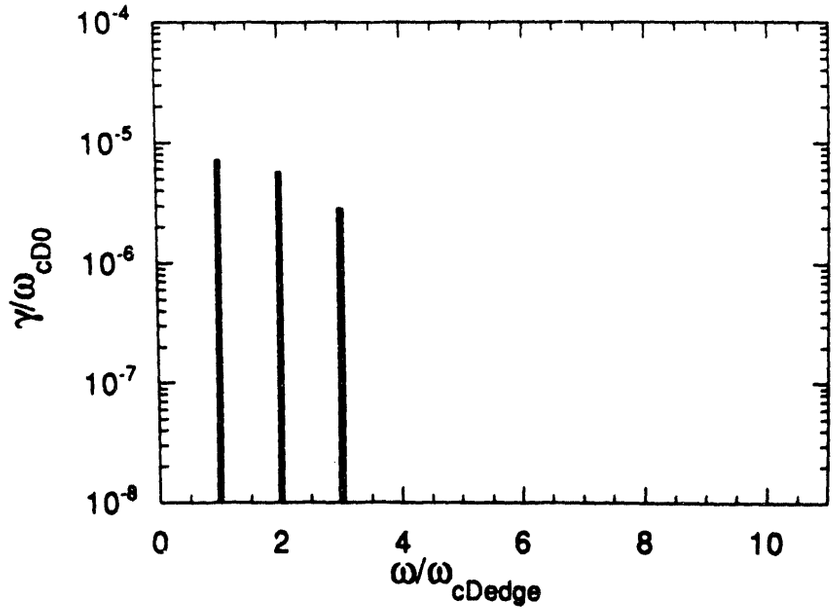
10-4
10-5
10-6
10-7
10-8
γ/ωcD0
0
2
4
6
8
10
ω/ωcDedge

Fig.3b.

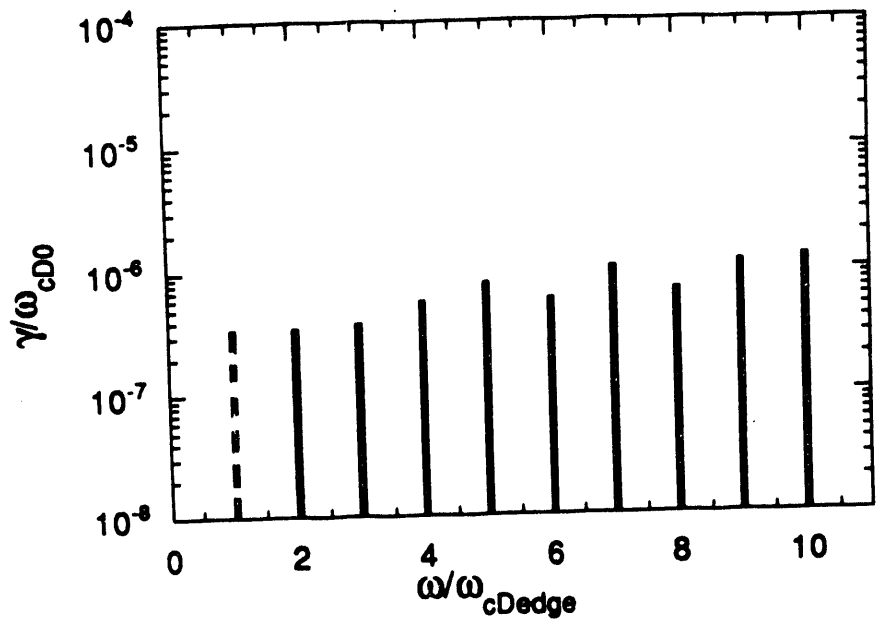
10^{-4}
10^{-5}
10^{-6}
10^{-7}
10^{-8}
γ/ω_{cD0}
0
2
4
6
8
10
ω/ω_{cDedge}

Fig.4 a.

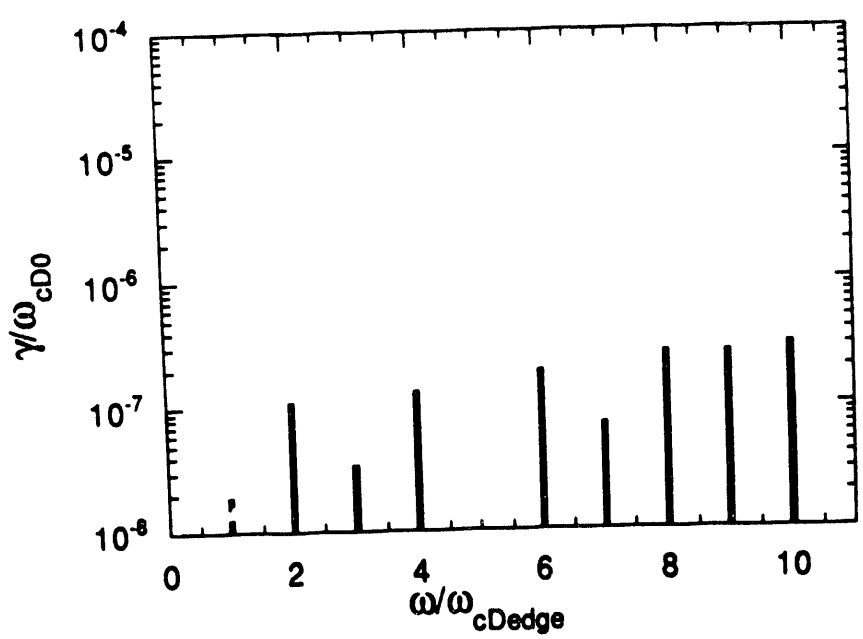
10^{-4}
10^{-5}
10^{-6}
10^{-7}
10^{-8}
γ/ω_{cD0}
0
2
4
6
8
10
ω/ω_{cDedge}

Fig.4b .

EXTERNAL DISTRIBUTION IN ADDITION TO UC-420

Dr. F. Paoloni, Univ. of Wollongong, AUSTRALIA
Prof. R.C. Cross, Univ. of Sydney, AUSTRALIA
Plasma Research Lab., Australian Nat. Univ., AUSTRALIA
Prof. I.R. Jones, Flinders Univ, AUSTRALIA
Prof. F. Cap, Inst. for Theoretical Physics, AUSTRIA
Prof. M. Heindler, Institut für Theoretische Physik, AUSTRIA
Prof. M. Goossens, Astronomisch Instituut, BELGIUM
Ecole Royale Militaire, Lab. de Phy. Plasmas, BELGIUM
Commission-European, DG. XII-Fusion Prog., BELGIUM
Prof. R. Boucique, Rijksuniversiteit Gent, BELGIUM
Dr. P.H. Sakanaka, Instituto Fisica, BRAZIL
Prof. Dr. I.C. Nascimento, Instituto Fisica, Sao Paulo, BRAZIL
Instituto Nacional De Pesquisas Espaciais-INPE, BRAZIL
Documents Office, Atomic Energy of Canada Ltd., CANADA
Ms. M. Morin, CCFM/Tokamak de Varennes, CANADA
Dr. M.P. Bachynski, MPB Technologies, Inc., CANADA
Dr. H.M. Skarsgard, Univ. of Saskatchewan, CANADA
Prof. J. Teichmann, Univ. of Montreal, CANADA
Prof. S.R. Sreenivasan, Univ. of Calgary, CANADA
Prof. R. Marchand, INRS-Energie et Materiaux, CANADA
Dr. R. Bolton, Centre canadien de fusion magnétique, CANADA
Dr. C.R. James,, Univ. of Alberta, CANADA
Dr. P. Lukác, Komenského Universzita, CZECHO-SLOVAKIA
The Librarian, Culham Laboratory, ENGLAND
Library, R61, Rutherford Appleton Laboratory, ENGLAND
Mrs. S.A. Hutchinson, JET Library, ENGLAND
Dr. S.C. Sharma, Univ. of South Pacific, FIJI ISLANDS
P. Mähönen, Univ. of Helsinki, FINLAND
Prof. M.N. Bussac, Ecole Polytechnique,, FRANCE
C. Mouttet, Lab. de Physique des Milieux Ionisés, FRANCE
J. Radet, CEN/CADARACHE - Bat 506, FRANCE
Prof. E. Economou, Univ. of Crete, GREECE
Ms. C. Rinni, Univ. of Ioannina, GREECE
Preprint Library, Hungarian Academy of Sci., HUNGARY
Dr. B. DasGupta, Saha Inst. of Nuclear Physics, INDIA
Dr. P. Kaw, Inst. for Plasma Research, INDIA
Dr. P. Rosenau, Israel Inst. of Technology, ISRAEL
Librarian, International Center for Theo Physics, ITALY
Miss C. De Palo, Associazione EURATOM-ENEA , ITALY
Dr. G. Grosso, Istituto di Fisica del Plasma, ITALY
Prof. G. Rostangni, Istituto Gas Ionizzati Del Cnr, ITALY
Dr. H. Yamato, Toshiba Res & Devel Center, JAPAN
Prof. I. Kawakami, Hiroshima Univ., JAPAN
Prof. K. Nishikawa, Hiroshima Univ., JAPAN
Librarian, Naka Fusion Research Establishment, JAERI, JAPAN
Director, Japan Atomic Energy Research Inst., JAPAN
Prof. S. Itoh, Kyushu Univ., JAPAN
Research Info. Ctr., National Instit. for Fusion Science, JAPAN
Prof. S. Tanaka, Kyoto Univ., JAPAN
Library, Kyoto Univ., JAPAN
Prof. N. Inoue, Univ. of Tokyo, JAPAN
Secretary, Plasma Section, Electrotechnical Lab., JAPAN
Dr. O. Mitarai, Kumamoto Inst. of Technology, JAPAN
Dr. G.S. Lee, Korea Basic Sci. Ctr., KOREA
J. Hyeon-Sook, Korea Atomic Energy Research Inst., KOREA
D.I. Choi, The Korea Adv. Inst. of Sci. & Tech., KOREA
Prof. B.S. Liley, Univ. of Waikato, NEW ZEALAND
Inst of Physics, Chinese Acad Sci PEOPLE'S REP. OF CHINA
Library, Inst. of Plasma Physics, PEOPLE'S REP. OF CHINA
Tsinghua Univ. Library, PEOPLE'S REPUBLIC OF CHINA
Z. Li, S.W. Inst Physics, PEOPLE'S REPUBLIC OF CHINA
Prof. J.A.C. Cabral, Instituto Superior Tecnico, PORTUGAL
Prof. M.A. Hellberg, Univ. of Natal, S. AFRICA
Prof. D.E. Kim, Pohang Inst. of Sci. & Tech., SO. KOREA
Prof. C.I.E.M.A.T, Fusion Division Library, SPAIN
Dr. L. Stenflo, Univ. of UMEA, SWEDEN
Library, Royal Inst. of Technology, SWEDEN
Prof. H. Wilhelmson, Chalmers Univ. of Tech., SWEDEN
Centre Phys. Des Plasmas, Ecole Polytech, SWITZERLAND
Bibliotheek, Inst. Voor Plasma-Fysica, THE NETHERLANDS
Asst. Prof. Dr. S. Cakir, Middle East Tech. Univ., TURKEY
Dr. V.A. Glukhikh,Sci. Res. Inst. Electrophys.I Apparatus, USSR
Dr. D.D. Ryutov, Siberian Branch of Academy of Sci., USSR
Dr. G.A. Eliseev, I.V. Kurchatov Inst., USSR
Librarian, The Ukr.SSR Academy of Sciences, USSR
Dr. L.M. Kovrizhnykh, Inst. of General Physics, USSR
Kernforschungsanlage GmbH, Zentralbibliothek, W. GERMANY
Bibliothek, Inst. Für Plasmaforschung, W. GERMANY
Prof. K. Schindler, Ruhr-Universität Bochum, W. GERMANY
Dr. F. Wagner, (ASDEX), Max-Planck-Institut, W. GERMANY
Librarian, Max-Planck-Institut, W. GERMANY

DATE
FILMED
9/6/94

END